Received: 7 January 2023 | Accepted: 11 January 2023 | Published on: 1 February 2023

DOI: 10.1002/asna.20230010

Astronomische Nachrichten

PROCEEDING

Structure and stability of differentially rotating compact stellar objects

Delaney Farrell[1] | **Rodrigo Negreiros**[2] | **Fridolin Weber**[1,3]

[1]Department of Physics, San Diego State University, San Diego, California, USA

[2]Instituto de Física, Universidade Federal Fluminense, Niterói, Brazil

[3]Center for Astrophysics and Space Sciences, University of California, San Diego, California, USA

Correspondence
Delaney Farrell, Department of Physics, San Diego State University, San Diego, CA, USA.
Email: dfarrell@sdsu.edu

Funding information
Conselho Nacional de Desenvolvimento Científico e Tecnológico; Coordenação de Aperfeiçoamento de Pessoal de Nível Superior; Fundação Carlos Chagas Filho de Amparo à Pesquisa do Estado do Rio de Janeiro; Instituto Nacional de Ciência e Tecnologia: Física Nuclear e Aplicações, Grant/Award Number: 464898/2014-5; National Science Foundation, Grant/Award Number: PHY-2012152

Abstract

Depending on the dynamics of a binary neutron star merger, the collision may result in a differentially rotating compact object. Differentially rotating stars can sustain a total mass considerably higher than that of a uniformly rotating star, giving rise to "hypermassive" objects like hypermassive neutron stars. These stars are likely to exhibit extreme structural deformation along the radial axis due to their high masses. Both the increased mass and structural deformations supported by differential rotation allow the compact remnant to remain stable in otherwise unstable configurations on short, dynamical timescales. In this work, we numerically simulate differentially rotating neutron stars to explore an increase in mass and structural deformation for three relativistic mean-field equations of state models. Results are used to predict outcomes for recent gravitational wave observations of binary neutron star mergers.

KEYWORDS

differential rotation, equation of state, neutron star

1 | INTRODUCTION

Neutron stars are the densest observed stellar objects, reaching supranuclear densities in their cores—up to an order of magnitude greater than nuclear saturation density. Because particles inside the star are squished together under immense pressure, the regions between the core and the crust of a neutron star are assumed to exist in a superfluid, frictionless state. Differential rotation occurs when these fluid-like regions that are adjacent at one point in time do not maintain that configuration; a star experiencing differential rotation will therefore have a rotational frequency that changes along the radial axis. Stars are most likely to experience a unique type of rotation, referred to as differential rotation, in extreme stellar events like binary star mergers. When a neutron star binary coalesces, the two stars are most likely irrotational just prior to merging (Galeazzi et al. 2012; Shapiro 2000). The collision would result in a substantial velocity discontinuity at the surface of contact, so the remnant star (a hypermassive neutron star, HMNS) left after the collision has a high likelihood of experiencing some degree of differential rotation. Neutron stars stabilized by differential rotation can sustain a total mass considerably

---

higher than that of a uniformly rotating star (Baiotti et al. 2008). These hypermassive neutron stars may also exhibit extreme deformation along the radial axis in the stabilization process. Rapid rotation and deformation of the star would result in a loss of angular momentum, which may provide an observable precursor before collapse (Cook et al. 1994). Both the increased mass and structural deformations supported by differential rotation allow the compact remnant to remain stable in otherwise unstable configurations on short, dynamical timescales. This is shown in the fully relativistic binary coalescence calculation of Shibata and Uryū (2000) where the stabilization on dynamic timescales (many milliseconds) of a compact remnant by differential rotation can lead to a delay in both the remnant's collapse and subsequent gravitational wave signal.

While the maximum mass and stabilization of differentially rotating neutron stars have been explored in the past (Morrison et al. 2004; Shapiro 2000), the astrophysics community has seen a stark revival of interest in the topic in the last few years. The renewed interest is largely due to a 2017 event where the Advanced Virgo and the two Advanced LIGO detectors observed a transient gravitational wave (GW) signal produced by the coalescence of a binary neutron star system (Abbott et al. 2017; Franceschetti et al. 2022). This event, GW170817, and the short gamma-ray burst that followed, GRB 180817A, marked the first observation of a neutron star binary merger event and a historic milestone for multi-messenger astronomy. One question remained after the event: what happened to the remnant left after the merger? The total mass of the merged remnant object was determined to be $M_{\mathrm{tot}}= 2.74^{+0.04}_{-0.01} M_{\odot}$, which is significantly larger than that of PSR J0952-0607, the heaviest well-observed neutron star mass $M = 2.35 \pm 0.17 M_{\odot}$. Beyond observation, the remnant's mass exceeds the maximum mass predicted by many popular equations of state models, leading researchers to believe the object eventually collapsed into a black hole. One hypothesis to explain the delayed collapse is the formation of a hypermassive neutron star (HMNS) supported on a short timescale by differential rotation. This hypothesis has been previously supported by full general relativistic simulations of both equal and unequal mass binaries for several equation of state (EOS) models.

We construct differentially rotating neutron stars for three different EOS models and tabulate their maximum allowed masses as a function of the degree of differential rotation. These mass values are used to predict the outcome of different binary neutron star merger events in Section 3.1. The structural deformation resulting from an increase in mass with rapid differential rotation is explored in Section 3.2.

2 | NUMERICAL MODEL

2.1 | Equilibrium model for differential rotation

Rotating neutron star calculations are performed in the framework of general relativity and depend on the matter's nuclear equation of state. Modeling rotating neutron stars is made complicated than spherically symmetric, non-rotating stars for a few reasons: rotation deforms neutron stars, stabilizes them against collapse, and drags along the local inertial frames inside and outside of them so that they co-rotate with the stars (Mellinger Jr et al. 2017). These rotational features must be included in the construction of the metric, which has the form

$$\begin{aligned} ds^2 = -e^{\gamma-\rho}dt^2 + e^{2\alpha}\left(dr^2 + r^2 d\theta\right) \\ + e^{\gamma-\rho} r^2 \sin^2\theta (d\phi - \omega dt)^2, \end{aligned} \tag{1}$$

where γ, ρ, α, and ω are metric functions dependent on the radial coordinate r and polar angle θ, and ω describes frame dragging due to rotation. These functions also implicitly depend on the star's angular velocity Ω. The metric functions are computed from Einstein's field equation

$$R^{\kappa\sigma} - \frac{1}{2} R g^{\kappa\sigma} = 8\pi T^{\kappa\sigma}, \tag{2}$$

where $R^{\kappa\sigma}$ is the Ricci tensor, R is the curvature scalar, and $g^{\kappa\sigma}$ is the metric tensor. $T^{\kappa\sigma}$ is the energy-momentum tensor given by

$$T^{\kappa\sigma} = (\varepsilon + P) u^{\kappa} u^{\sigma} + g^{\kappa\sigma} P, \tag{3}$$

where ε and P are supplied by the equation of state. Solving for the gravitational field equations is as follows. Three of the four metric potentials ρ, γ, and ω, are expressed using Green's functions (see Appendix A in Cook et al. (1994) for full derivation). The fourth gravitational field α reduces to a linear ordinary differential equation.

Once the metric functions are solved for, they are used to solve the equation of hydrostatic equilibrium for a barotropic fluid:

$$h(P) - h_p = \frac{1}{2}\left[\gamma_p + \rho_p - \gamma - \rho - \ln\left(1 - v^2\right) + F(\Omega)\right] \tag{4}$$

where $h(P)$ is the enthalpy as a function of pressure, γ_p, and ρ_p are the values of the metric potentials at the pole. The quantity v is defined as

$$v = (\Omega - \omega) r \sin \theta e^{-\rho}, \tag{5}$$

and the last term, $F(\Omega)$, defines the rotational law for the matter. Following the form in Cook et al. (1992), Cook et al. (1994), and Komatsu et al. (1989) we set this function to

$$F(\Omega) = A^2 \left(\Omega_c - \Omega\right), \tag{6}$$

where Ω_c is the central value for the angular velocity. The parameter A is a constant scaling factor of the degree of differential rotation and is used to determine the length scale over which the frequency changes (Morrison et al. 2004). Note that uniform rotation is achieved in the limit $d\Omega = 0$, or as $A^{-1} \to 0$. The particular rotation law is advantageous to adopt for two reasons. The first is that this form is widely used throughout literature, so using the same rotation law ensures our work can be compared with others. The second is previous work suggests the above law provides a reasonable parameterization of differential rotation profiles expected in binary neutron star merger remnants, of which observational data is rapidly growing (Morrison et al. 2004).

Simplifying Equation (4) and including the rotation law gives

$$(\Omega_c - \Omega) = \frac{1}{A^2}\left[\frac{(\Omega - \omega)s^2\left(1 - \mu^2\right)e^{-2\rho}}{(1 - s)^2 - (\Omega - \omega)^2 s^2\left(1 - \mu^2\right)e^{-2\rho}}\right], \tag{7}$$

where the rotational frequency Ω can be isolated and solved numerically using a root-finding algorithm. The other non-defined parameters, s and μ, represent the radial and polar coordinates. The gravitational and matter fields are solved on a discrete grid with a computational domain in r and θ space. Following Cook et al. (1992), we redefine these coordinates to s and μ as

$$r = r_e\left(\frac{s}{1 - s}\right), \tag{8}$$

where r_e is the equatorial radius and

$$\mu = \cos\theta. \tag{9}$$

Calculations are done on the computational domain $0 \leq s \leq 1$ and $0 \leq \mu \leq 1$. Once a set of self-consistent solutions to these equations is obtained, physical quantities like mass, angular momentum, and rotational kinetic energy are outputted.

An iterative method is employed to solve the four field equations, ρ, γ, ω, and α, and the integrated equation of hydrostatic equilibrium, Equation (4). In the iterative scheme, all values are redefined to be unit-less (see Cook et al. (1992) for the full list of redefined quantities), allowing the second-derivative terms to be rewritten as flat-space derivative operators; these flat-space operators are then inverted in the scheme by using explicit flat-space Green's functions. First and second-order derivatives are approximated with a standard three-point formula. The discrete grid is 329×125 (radial × angular), and because of the coordinate transformation in Equations (8) and (9), the integration domain is all space ($0 \leq r \leq \infty$). The modification to include differential rotation uses Equation (6) as the specified rotation law. Rotational frequency, therefore, is updated from a constant to a vector dependent on the radius, and is obtained by finding a solution to a set of coupled non-linear equations; for this solution, we use Newton–Raphson with second-order convergence (Janicke and Kost 1998).

Given an EOS and a specified value of rotation parameter A, the above numerical procedure is used to construct single star and sequences of models either with constant central densities or constant baryon numbers.

2.2 | Equation of state

The algorithm *DRNS* requires a tabulated equation of the state model as an input. The three nuclear EOS models discussed in this work are variations of the relativistic mean-field model GM1L constructed at zero temperature. Each variation, dubbed GM1L_b, GM1L_c, and GM1L_f, varies in particle composition demonstrated in Table 1.

TABLE 1 Particle composition for different variations of the GM1L equation of state model. The • indicates the particle is present, while the – indicates the particle is not accounted for.

Model	p	n	Σ	Λ	Ξ	Δ	e^-	μ^-
GM1L_b	•	•	•	•	•	•	•	•
GM1L_c	•	•	–	–	–	–	•	•
GM1L_f	•	•	•	•	•	•	•	•

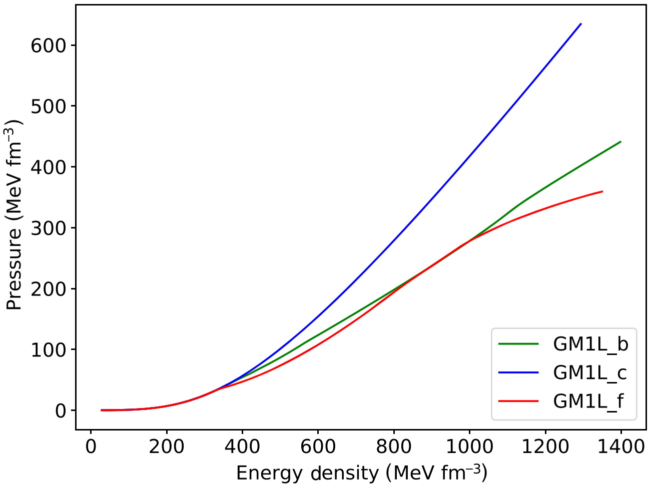

FIGURE 1 Pressure versus energy density of the three variations of GM1L used in computation: GM1L_b, GM1L_c, and GM1L_f

GM1L_c only accounts for protons and neutrons (with electrons and muons included for chemical equilibrium). Models GM1L_b and GM1L_f include all particles of the baryon octet and all four electrically charged states of the $\Delta(1232)$ isobar. The three variations are shown visually in Figure 1. The GM1L_c model yields the largest pressure of all three equations of state since hyperons and the Δ isobar do not contribute in this case. The pressure of the GM1L_b model exceeds that of GM1L_f, which has its origin in the larger meson–Δ isobar couplings, that is, $g_{\sigma\Delta} = 1.2 g_{\sigma N}$, $g_{\omega\Delta} = 1.2 g_{\omega N}$, $g_{\rho\Delta} = 1.2 g_{\rho N}$, compared to $g_{\sigma\Delta} = 0.8 g_{\sigma N}$, $g_{\omega\Delta} = 0.8 g_{\omega N}$, $g_{\rho\Delta} = 0.8 g_{\rho N}$ for GM1L_f.

3 | RESULTS

We demonstrate results for stellar sequences and individual stellar models from *DRNS* created with the three EOS models GM1L_b, GM1L_c, and GM1L_f. For stellar sequences, we compare maximum gravitational mass values with varying degrees of differential rotation to uniform and non-rotating results. Additionally, individual stellar maps are constructed for extreme cases of differential rotation to highlight structural deformation from spherical symmetry.

3.1 | Stellar Sequences: Maximum Mass

We construct stellar sequences of differentially rotating, relativistic neutron stars for three different EOS models. Because the rotation parameter A repeatedly appears as A^{-1} in the equations described in Section 2, we follow the lead of previous work which parameterized sequences by values of $A^{-1} = 0.3, 0.5, 0.7,$ and 1.0 (Cook et al. 1992; Galeazzi et al. 2012; Morrison et al. 2004). Maximum gravitational mass values for varying degrees of differential rotation (M^{DIF}), as well as for uniform rotation at the Kepler frequency (M^{UNI}) and for Tolman-Oppenheimer-Volkoff results (M^{TOV}), are given for all three EOS models in Table 2 and shown visually for GM1L_b in Figure 2. We see an increase in mass as A^{-1} increases in all cases except for GM1L_c; only $A^{-1} = 1.0$ does not follow this trend.

TABLE 2 Maximum gravitational mass configurations for GM1L_b, GM1L_c, and GM1L_f. Tolman-Oppenheimer-Volkoff (TOV) is zero rotation, UNI is uniform rotation at the Kepler frequency, and DIF is differential rotation. All masses are given in units of $M_\odot$.

Mass	GM1L_b	GM1L_c	GM1L_f
M^{TOV}	2.025	2.295	1.928
M^{UNI}	2.346	2.630	2.232
$M^{DIF}, A^{-1} = 0.3$	2.088	2.572	1.985
$M^{DIF}, A^{-1} = 0.5$	2.500	3.205	2.353
$M^{DIF}, A^{-1} = 0.7$	2.945	3.719	2.733
$M^{DIF}, A^{-1} = 1.0$	3.457	2.399	3.244

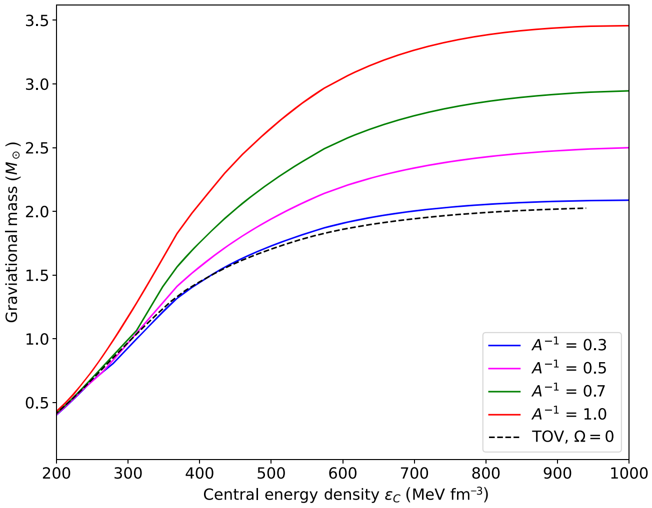

FIGURE 2 Mass versus central density relations from equation of state (EOS) GM1L_b. Solid-colored lines depict varying values of A^{-1} compared to a dashed black line depicting Tolman-Oppenheimer-Volkoff (TOV) results (no rotation).

Comparing maximum masses from the non-rotating TOV curves to the maximum masses from differential rotation curves, GM1L_b shows an increase of 70.7%, GM1L_c shows an increase of 62%, and GM1L_b shows an increase of 68.25%. This is a sizable increase compared to uniform rotation, which increases the maximum mass set by the Kepler limit by roughly 20% when compared to the maximum mass in non-rotating simulations (Lyford et al. 2003).

As stated previously, differential rotation is one of the mechanisms which stabilizes a remnant star after a binary neutron star merger. This remnant star may take on several different forms depending on the dynamics of the merging system, as well as the stars' underlying nuclear EOS—a still relatively unknown relationship (Radice et al. 2020). A good estimate of the fate of the event comes from the total mass of the two merging stars, a value which can now be determined with high accuracy from new detectors like Advanced LIGO and Virgo. A neutron star binary can result in the formation of a black hole (BH), a supermassive neutron star (SNS), or a hypermassive neutron star (HMNS). A remnant SNS or HMNS may be "short-lived," where the remnant collapses within 10–20 ms of the merger, or long-lived, evolving into a more stable configuration in ≥20 ms. For very massive systems, the outcome is likely the prompt formation of a black hole. BH formation is likely if the total rest mass of the system is greater than M^{DIF} (Morrison et al. 2004), or if the rest mass of the remnant is greater or equal to $M_{thr} = k_{thr}M^{TOV}$ where k_{thr} is a scaling factor = 1.3 to 1.7 dependent on the underlying system's EOS (Radice et al. 2020). An HMNS is likely to form if the system's rest mass is greater than the mass limit set by uniform rotation, M^{UNI}, but less than M^{DIF}. And finally, an SNS is likely to occur if total rest mass is greater than the mass limit set by TOV calculations (no rotation), M^{TOV}, but less than uniform rotation M^{UNI}.

While comparing theoretical masses as guidelines for the possible fates of neutron star binary mergers gives a good estimate, it is important to note other factors like finite temperatures and spins might also affect the merger outcome (Radice et al. 2020). Regardless, it is safe to assume the underlying EOS greatly influences the fate of the compact remnant. We compare the maximum masses for the three versions of GM1L found in Table 2 with the total mass of three neutron star binary observations. The first is GW170817, the first neutron star binary merger detected by gravitational wave (GW) emission in 2017 from the Advanced LIGO and Virgo collaboration (B. P. Abbott et al. 2017). The second is GW190425, the heaviest binary neutron star system to be detected (B. Abbott et al. 2020). And the last is the double pulsar binary J0737-3039, one of the lightest binary systems ever observed (Podsiadlowski et al. 2005). The compact remnant's potential form (BH, SNS, and HMNS) of each binary system is predicted from each of the three EOS models, shown in Table 3. For both EOS models GM1L_b and GM1L_c, all three mergers could potentially form an HMNS, which is likely to collapse into a BH for the higher mass binary systems. GM1L_f predicts a prompt collapse for both GW observations; their confidence intervals are shown visually in Figure 3. Table 3 reinforces that the outcome of a neutron star binary coalescence is sensitive to the underlying EOS and that the observation of such events is a promising avenue to place constraints on our knowledge of the nuclear EOS of neutron star matter.

TABLE 3 Possible outcomes (black hole [BH], supermassive neutron star [SNS], or hypermassive neutron star [HMNS]) of binary neutron star mergers based on calculations from GM1L_b, GM1L_c, and GM1L_f (shown as **b**, **c**, and **f**, respectively). All masses are given in $M_\odot$. See text for more details.

Observation	Total Mass	b	c	f
GW170817	$2.74^{+0.04}_{-0.01}$	HMNS	HMNS	BH
GW190425	$3.4^{+0.3}_{-0.1}$	HMNS	HMNS	BH
J0737-3039	$2.59^{+0.003}_{-0.003}$	HMNS	SNS	HMNS

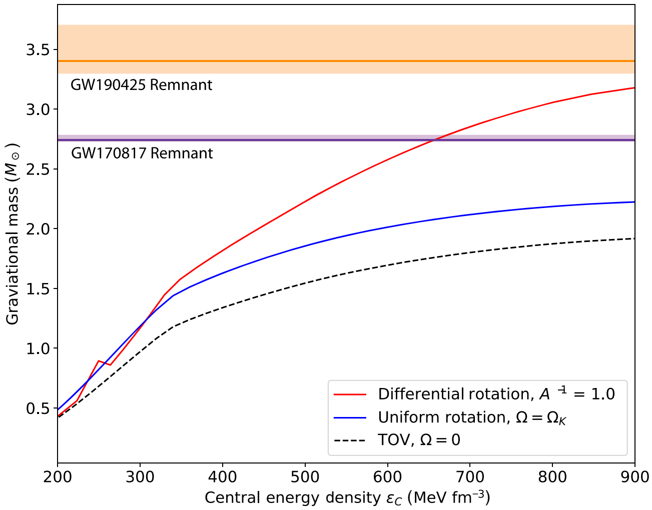

FIGURE 3 Mass versus central density relations from equation of state (EOS) GM1L_f, comparing differential rotation with $A^{-1} = 1.0$ to uniform rotation and Tolman-Oppenheimer-Volkoff (TOV) (no rotation) results. The purple horizontal bar shows the mass confidence interval for the remnant of GW170817, and the orange horizontal bar shows the mass confidence interval for the remnant of GW190425. See text for more details.

3.2 | Individual models: structural deformation

Beyond stellar sequences, we construct energy density maps to explore how differential rotation impacts the structure of a neutron star. Rapid uniform rotation is shown to cause the shape of a star to deviate from spherical symmetry, where the star flattens at the pole and widens in the equatorial direction (Weber 2017). Differential rotation should cause a similar type of structural deformation, but likely more exaggerated; recent results from Gondek-Rosiska et al. (2017) depict a torus-like shape for extreme cases of differential rotation. We present cross-sections of individual stellar models constructed from the EOS GM1L_c, comparing deformation for four values of A^{-1}. As shown in Figure 4, as A^{-1} increases, the greater the deviation from a spherical shape. Results are shown for polar to equatorial radius ratio $r_p/r_e = 0.6$, with central densities of 800 MeV fm^{-3}.

To achieve a fully toroidal structure, the ratio r_p/r_e would need to tend to zero. For the three EOS models tested, described numerical scheme failed to produce physical results with $r_p/r_e \leq 0.5$, meaning the most extreme configurations calculated were just beginning to appear "quasi-toroidal," in which the maximal density is not the central one, as shown in the bottom right panel of Figure 4. The constraint on the ratio $r_p/r_e \leq$

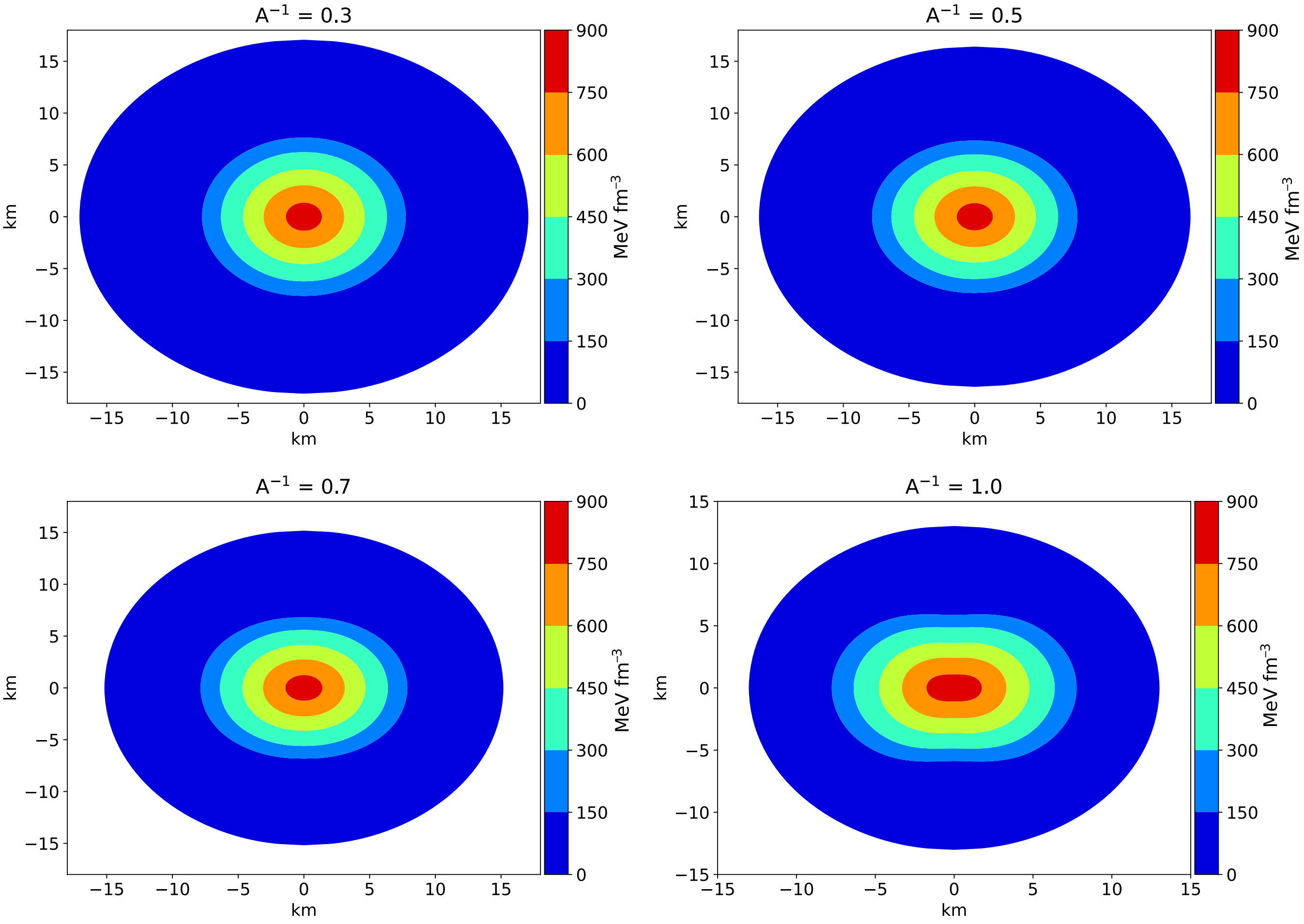

FIGURE 4 Energy density (in MeV fm^{-3}) cross sections of individual stellar models from equation of state (EOS) GM1L_c, comparing differential rotation with $A^{-1} = 0.3$ (top left), 0.5 (top right), 0.7 (bottom left), and 1.0 (bottom right)

arises from numerical instability and not from the underlying EOS model, so we expect fully toroidal results in the future.

4 | CONCLUSIONS

In this work, we compare the results of differentially rotating stellar sequences and individual stellar models resulting from three EOS models: GM1L_b, GM1L_c, and GM1L_f. The three EOS models see an average increase in maximum gravitational mass from TOV results of 67%, with masses $> 3M_{\odot}$ achieved for all three models as shown in Section 3.1. Maximum mass values are then used to predict the outcome of two binary neutron star merger events, GW170817 and GW190425, as well as the low-mass binary system J0737-3039. In Section 3.2, cross-sections of energy density from individual stellar models with varying degrees of differential rotation are discussed for GM1L_c. As shown in Figure 4, increasing differential rotation flattens the star at the pole and widens in the equatorial direction as with uniform rotation. For the highest value of the rotation parameter A^{-1}, the cross-section of energy density indicates the structure of the star tends toward a quasi-toroidal configuration.

The results presented are limited by a numerical instability introduced as the polar-to-equatorial radius ratio tends toward zero; we expect to address this issue in the future. Additionally, the three EOS models used are all constructed at zero temperature, but temperature plays an important role in the outcome of binary neutron star merger events. Further work will explore the application of finite temperature EOS models to the algorithm *DRNS*.

ACKNOWLEDGMENTS

Delaney Farrell and Fridolin Weber are supported by the National Science Foundation (USA) under Grant No. PHY-2012152. Rodrigo Negreiros acknowledges financial support from CAPES, CNPq, and FAPERJ. This work is part of the project INCT-FNA (No. 464898/2014-5) as well as FAPERJ JCNE.

ORCID

Delaney Farrell https://orcid.org/0000-0003-1512-712X

REFERENCES

Abbott, B. P., Abbott, R., Abbott, T., et al. 2017, *Phys. Rev. Lett.*, *119*(16), 161101.

Abbott, B., Abbott, R., Abbott, T., et al. 2020, *Astrophys. J. Lett.*, *892*(1), L3.

Baiotti, L., Giacomazzo, B., & Rezzolla, L. 2008, *Phys. Rev. D*, *78*(8), 084033.

Cook, G. B., Shapiro, S. L., & Teukolsky, S. A. 1992, *Astrophys. J.*, *398*, 203.

Cook, G. B., Shapiro, S. L., & Teukolsky, S. A. 1994, *Astrophys. J.*, *424*, 823.

Franceschetti, K., Del Zanna, L., Soldateschi, J., & Bucciantini, N. 2022, *Universe*, *8*(3), 172.

Galeazzi, F., Yoshida, S., & Eriguchi, Y. 2012, *Astronom. Astrophys.*, *541*, A156.

Gondek-Rosi«ska, D., Kowalska, I., Villain, L., Ansorg, M., & Kucaba, M. 2017, *Astrophys. J.*, *837*(1), 58.

Janicke, L., & Kost, A. 1998, *IEEE Trans. Magn.*, *34*(5), 2505.

Komatsu, H., Eriguchi, Y., & Hachisu, I. 1989, *Mon. Not. R. Astronom. Soc.*, *237*(2), 355.

Lyford, N. D., Baumgarte, T. W., & Shapiro, S. L. 2003, *Astrophys. J.*, *583*(1), 410.

Mellinger, R. D. Jr., Weber, F., Spinella, W., Contrera, G. A., & Orsaria, M. G. 2017, *Universe*, *3*(1), 5.

Morrison, I. A., Baumgarte, T. W., & Shapiro, S. L. 2004, *Astrophys. J.*, *610*(2), 941.

Podsiadlowski, P., Dewi, J., Lesaffre, P., Miller, J., Newton, W., & Stone, J. R. 2005, *Mon. Not. R. Astronom. Soc.*, *361*(4), 1243.

Radice, D., Bernuzzi, S., & Perego, A. 2020, *Annu. Rev. Nucl. Part. Sci.*, *70*, 95.

Shapiro, S. L. 2000, *Astrophys. J.*, *544*(1), 397.

Shibata, M., & Uryū, K. 2000, *Phys. Rev. D*, *61*(6), 064001.

Weber, F. 1999, *Pulsars as Astrophysical Laboratories for Nuclear and Particle Physics*, IOP Publishing (Bristol, Great Britain).

AUTHOR BIOGRAPHY

Delaney Farrell is a PhD candidate in computational science at San Diego State University and the University of California, Irvine. She recieved her bachelor's degree in physics at San Diego State University. She is interested in neutron stars, dense matter, and computational astrophysics.

How to cite this article: Farrell, D., Negreiros, R., & Weber, F. 2023, *Astron. Nachr.*, *344*, e230010. https://doi.org/10.1002/asna.20230010